ACS NANO

www.acsnano.org

ARTICLE

Twisted Light-Enhanced Photovoltaic Effect

Kristan Bryan Simbulan, Yi-Jie Feng, Wen-Hao Chang, Chun-I Lu, Ting-Hua Lu,* and Yann-Wen Lan*

Cite This: *ACS Nano* 2021, 15, 14822–14829

Read Online

ACCESS | Metrics & More | Article Recommendations | Supporting Information

ABSTRACT: Twisted light carries a defined orbital angular momentum (OAM) that can enhance forbidden transitions in atoms and even semiconductors. Such attributes can possibly lead to enhancements of the material's photogenerated carriers through improved absorption of incident light photons. The interaction of twisted light and photovoltaic material is, thus, worth studying as more efficient photovoltaic cells are essential these days due to the need for reliable and sustainable energy sources. Two-dimensional (2D) MoS_2, with its favorable optoelectronic properties, is a good platform to investigate the effects of twisted light on the photon absorption efficiency of the interacting material. This work, therefore, used twisted light as the exciting light source onto a MoS_2 photovoltaic device. We observed that while incrementing the incident light's quantized OAM at fixed optical power, there are apparent improvements in the device's open-circuit voltage (V_{OC}) and short-circuit current (I_{SC}), implying enhancements of the photoresponse. We attribute these enhancements to the OAM of light that has facilitated improved optical absorption efficiency in MoS_2. This study proposes a way of unlocking the potentials of 2D-MoS_2 and envisions the employment of light's OAM for future energy device applications.

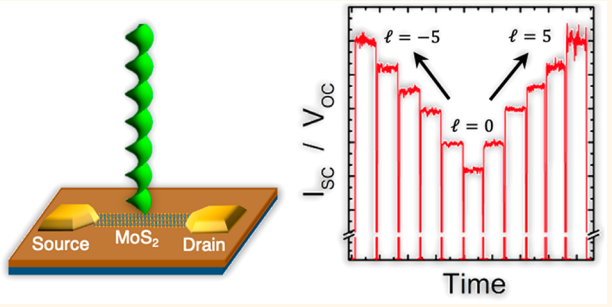

KEYWORDS: *enhanced photovoltaic effect, twisted light, orbital angular momentum, molybdenum disulfide, solar cell, photoresponse*

INTRODUCTION

State-of-the-art light-emitting diodes, phototransistors, and solar cells are a few of the optoelectronic devices that have been instrumental in further technological advancements in robotics, energy harvesting, and healthcare, among others. In particular, solar or photovoltaic cells offer sustainable energy that can be used as an effective alternative to the progressively depleting conventional energy sources, such as coal, natural gas, and crude oil. Furthermore, since solar radiation is available almost everywhere, solar panels can be installed ubiquitously, significantly reducing power losses due to transmission. However, despite this advantage, challenges regarding power conversion efficiency (PCE) are still faced by the latest photovoltaic cell technology. The highest PCE recorded to date is about 47% using multijunction concentrator solar cells,[1] but the majority of photovoltaic cells in the market have modular efficiencies below 21%.[2] Hence, academic and industry researchers continue to find innovative ways to improve cell efficiency and make photovoltaic technology more affordable for everyone.

Light is the essential driving source for photovoltaic cells as it is for other optoelectronic devices. Photons of light striking a semiconductor and absorbed by the charge carriers may lead to electronic transitions that create photogenerated carriers, enhancing the material's conductivity. Optical tuning of the electrical conductivity was conventionally carried out by varying the incident light's intensity and frequency. However, recently, other properties of light have been discovered to cause selective carrier excitations, which can possibly affect the level of photogenerated carriers. The spin angular momentum (SAM) of circularly polarized light has been shown to prioritize certain transition states in the Γ-point of a GaAs crystal[3,4] and selectively excite carriers in either the K or K' valley of monolayer transition metal dichalcogenides (TMDCs).[5] SAM utilizes the two circular polarization states of light—left-handed and right-handed, as it introduces an additional degree of freedom. Another property of light, which is recently gaining much attention, is its orbital angular momentum (OAM). Light with OAM, also called *twisted light*, carries a well-defined OAM of $l\hbar$ per photon,[6] where its topological charge l can take thousands of possible integer values or states.[7] In previous studies, twisted light carrying different OAM have been employed in varying the levels of light-generated electron signals in GaAs,[8] which was attributed to the electrons that are excited through the OAM-of-light-

Received: June 9, 2021
Accepted: August 24, 2021
Published: August 26, 2021

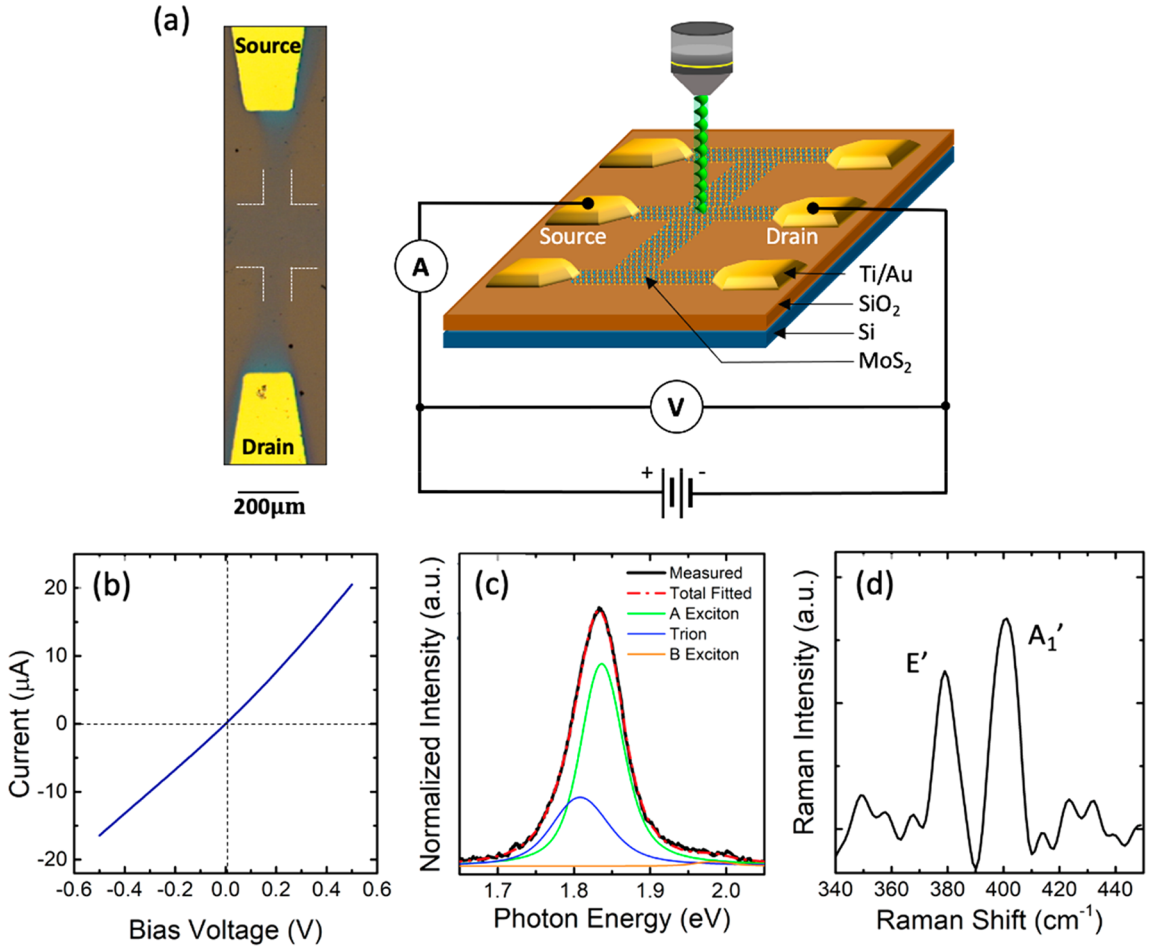

Figure 1. Device structure and characteristics. (a) Left: optical image of the monolayer MoS_2 channel device (the middle channel is shown); Right: diagram of the whole device and the measurement setup. (b) The current−voltage curve in dark condition, evidencing the existing *p-n* junction in the device (c) PL and (d) Raman spectra of the MoS_2 channel. The PL spectra consists of three dominant peaks: The A and B excitons (~150 meV apart) and the trion (~30 meV away from the A exciton).

enhanced quadrupole transitions.[9−12] Likewise, twisted light has also been demonstrated to have induced *l*-dependent photocurrents in thin WTe_2 photodetectors.[13] It is therefore apparent that, like circularly polarized light, twisted light can offer an additional degree of freedom. Its large number of OAM states allows a broader control of which transition states will be accessible.[9] This implies that an enhanced photon absorption and photogeneration of carriers in semiconductors may be achieved owing to these additional light-enhanced transition channels. The interaction of twisted light with different materials, particularly photovoltaic materials, is thus worth investigating as this may yield to improvements in photovoltaic properties and absorption efficiency, a step toward an improved solar cell efficiency.

The attractive properties of monolayer TMDCs, for example, strong spin−orbit coupling, optical bandgap in the visible range, and impressive optical sensitivity on a thickness for thickness comparison, have made them a good platform for studying the potentials of the twisted light in enhancing absorption efficiency for photovoltaic devices. Monolayer molybdenum disulfide (MoS_2)—a prototypical TMDC—has been one of the subjects of many researchers in terms of developments of ultrathin and flexible photovoltaic devices. Well performing MoS_2 solar cells have been reported with both heterojunction[14−16] and homojunction[17−20] structures, offering advantages of structural flexibility, high PCE,[16] simplicity of structure,[17] and applicability with Si-based electronics technology.[14] Single-layer MoS_2 has a considerably large absorption coefficient,[21,22] in the order of 10^6 cm^{-1}, compared to that of silicon (~10^4 cm^{-1} at 532 nm and 300 K),[23] which is indeed an advantage for energy harvesting applications. However, due to its atomic thickness, the absorption of incident photons is only limited to ~11%.[24] Hence, device structural changes were implemented in recent MoS_2 devices to achieve better absorption.[25−27] Nevertheless, insofar as our knowledge is concerned, there have been no methods reported yet that exhibit enhanced absorption in MoS_2 by varying the structural properties of the incident light.

In this work, we excited a single-layer MoS_2 channel, exhibiting photovoltaic properties, with twisted light. In our experiments, we have observed improvements in the open circuit voltages (V_{OC}) and short-circuit currents (I_{SC}), across the MoS_2 device, after illumination of twisted light. Specifically, at fixed laser power, the levels of the I_{SC} and the V_{OC} follow an increasing pattern along with the *l* of light. This is further supported by photoluminescence (PL) measurements through the corresponding trion and exciton intensities trends with respect to *l* and under a strictly fixed excitation power, as well as power-dependent electrical measurements. The use of structured light, therefore, may offer an easy addition, or yet,

https://doi.org/10.1021/acsnano.1c04902
ACS Nano 2021, 15, 14822−14829

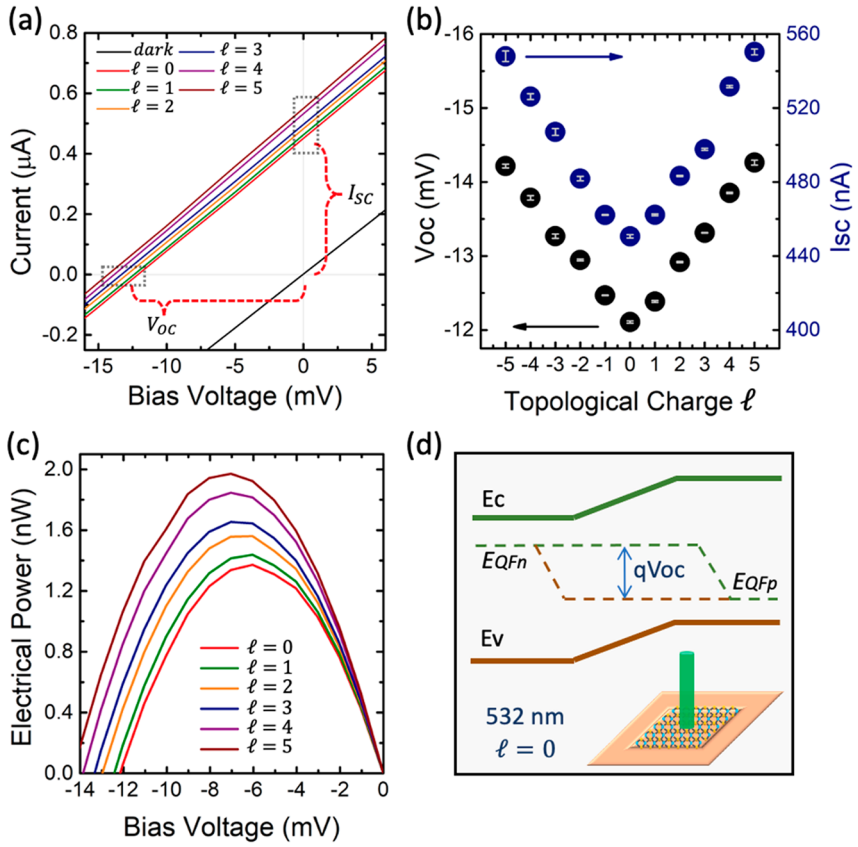

Figure 2. Enhancement of the photovoltaic effect in monolayer MoS_2. (a) Drain-source current versus bias voltage (I–V) characteristic of the device under dark and under illumination of light carrying different l (20 μW laser power, 532 nm wavelength); $l = 0$ refers to the fundamental mode beam. (b) The corresponding short-circuit currents (I_{SC}) and open-circuit voltages (V_{OC}) at various l conditions, and the (c) generated electrical power versus bias voltage of the device as extracted from its characteristic curve in (a). The error bars in (b) are derived from three different measurements in each measurement condition. (d) The photovoltaic mechanism in an illuminated *p*-*n* junction device.

an alternative to the already existing means of enhancing the photovoltaic properties of energy harvesting devices.

RESULTS/DISCUSSION

Nonuniform defect distributions in chemical vapor deposition-grown (CVD-grown) MoS_2 semiconductors have induced different doping concentrations at various areas of the material.[20,28] Such structural irregularity is consistent with the reported characteristics of CVD-grown MoS_2,[29] where varying proportions of sulfurization of MoO_3 have caused varying amounts of defects within the crystal and may have led to several n and n^+ (higher n-doped) regions forming *p*-*n* junctions. Thus, to form *p*-*n* homojunctions in our device channel, CVD with similar parameters was intentionally used to grow the single-layer continuous MoS_2 on a ∼90 nm thick SiO_2 on Si substrate. It was then etched in Argon plasma to form the channels before depositing onto it the Ti (20 nm)/Au (80 nm) source and drain electrodes, as shown in Figure 1(a). The AFM profile of the MoS_2 channel is likewise displayed in Supporting Information (SI) Figure S1, evidencing a single layered structure. The completed device is a Hall bar structure and consists of three parallel channels of almost equal dimensions. All two-terminal electrical measurements were performed on the device using the parameters specified in the Methods section. Consequently, direct current measurements between the device's source and drain terminals show, as expected, the presence of a *p*-*n* junction, signaling a small rectification evidenced in Figure 1(b). Meanwhile, all optical measurements were recorded from the device via a micro-Raman spectroscopy setup. A spatial light modulator (SLM) was inserted along the optical path to provide an option to convert an incident 532 nm Gaussian beam ($l = 0$) into a twisted light ($l \neq 0$). The radial indices of the generated twisted light were all set to zero. The simplified diagram of the optical setup is shown in SI Figure S2, along with the beam spot images of light with selected values of l. An incident fundamental light ($l = 0$) impinges the sample through a 50× objective lens (NA = 0.50) and nonresonantly ($E_{photon} > E_{gap}$) excites the MoS_2 channel, resulting in a PL spectrum (Figure 1(c)) composed of three dominant peaks. These peaks were identified as contributions by the A excitons (∼1.837 eV), B excitons (∼1.98 eV), and negative trions (∼1.80 eV).[30,31] Raman measurements of the device channel (Figure 1(d)), on the other hand, showed the two dominant phonon modes of MoS_2.[30,32] Fixed optical power (P_{laser}) was used in each set of measurements to ensure that the corresponding analysis were based on the fact that almost consistent amount of photons per unit time goes to the sample.

The device's photoresponse was measured while illuminated with incident light of varying OAM ($l\hbar$), including zero OAM, almost exactly at the center of the middle channel, as demonstrated in the right image of Figure 1(a). Illuminating far from the metal electrodes and at the center of the channel prevents any unintended contributions from photothermo-

https://doi.org/10.1021/acsnano.1c04902
ACS Nano 2021, 15, 14822−14829

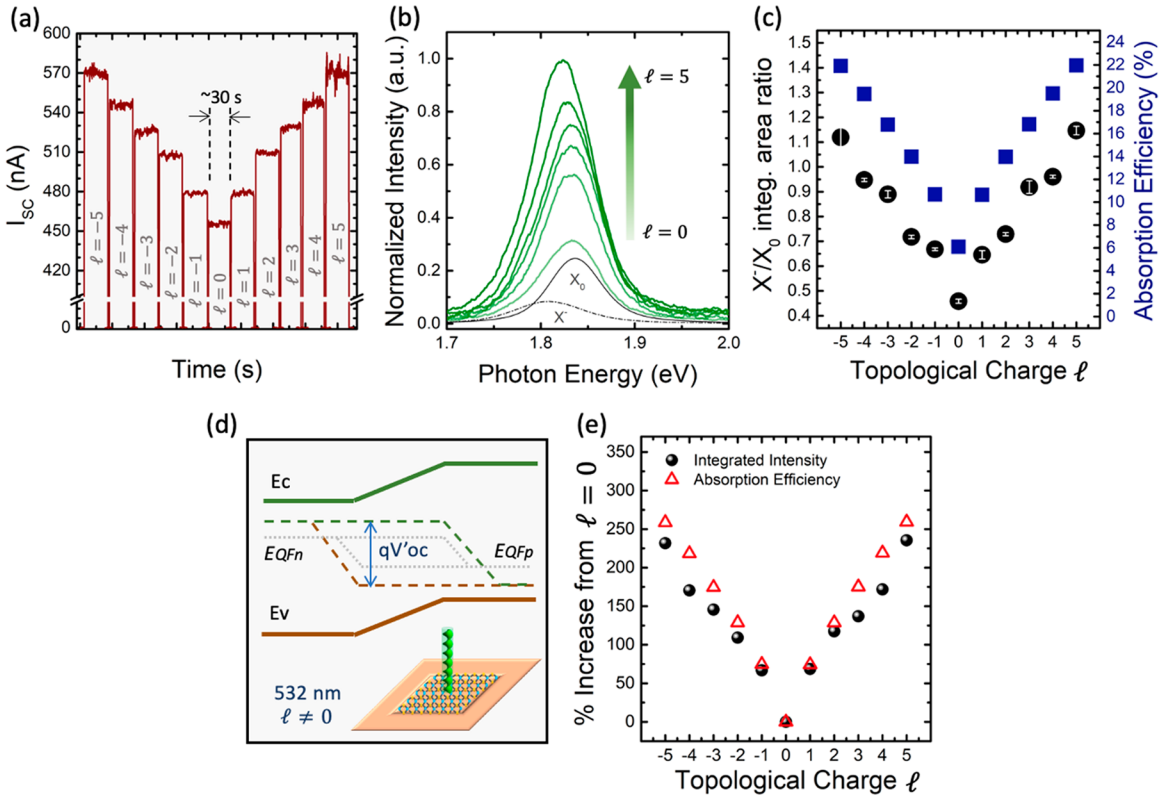

Figure 3. Simultaneous optical and electrical measurement. (a) Drain-source current versus time (I-T) curve recorded simultaneously with the (b) Photoluminescence (PL) spectra of the monolayer MoS_2 device illuminated by incident light with different values of l and fixed laser power (20 μW). Only the fitted exciton and trion peaks for $l = 0$ is shown in (b) to tidy up the graph. (c) Left axis: The ratio of the spectral area of the trion and A exciton peaks (X^-/X_0) corresponding to the PL spectrum in (b) indicated by l. The error bars show the deviations of the X^-/X_0 among three consecutive spectral measurements. Right axis: The estimated absorption efficiency at given values of l of the incident light. (d) Comparison of the quasi-Fermi levels induced at $l \neq 0$ condition versus that of $l = 0$ (gray dotted lines). (e) The percent increase of both the PL integrated intensity and the absorption efficiency at different measurement conditions relative to that of $l = 0$ condition.

electric and photovoltaic effects in the MoS_2-metal interface.[33] Three consecutive $I-V$ characteristics were then measured for every value of the incident light's l at a fixed power of 20 μW on the sample side. A representative curve for each light condition is shown in Figure 2(a). Also, to avoid prolonged heating on the sample, a long ~5 min break was imposed in-between measurements. The apparent I_{SC} and V_{OC} (Figure 2(b)) vary almost linearly with the l of the incident light, with I_{SC} increasing by ~100 nA and V_{OC} rising by ~2 mV from $l = 0$ to$l = 5$. The generated electrical power (Figure 2(c)) consequently improves by ~1.5% from 1.4 nW at $l = 0$ to 2.0 nW at $l = 5$. Figure 2(a),(c) only show the results for the case of the incident light with positive $l\hbar$, the data set for that of the negative $l\hbar$ are presented in SI Figure S3. The nearly symmetrical relationship between these two data sets implies that a similar mechanism occurs regardless of the OAM's sign. Furthermore, SI Figure S4 contains another set of results from the same device recorded with a fixed power of 100 μW. The observed behavior therein is consistent with that of the above results but with higher V_{OC} and I_{SC} levels due to the larger exciting power. The same behavior is also obtained at fixed 100 μW optical power from a second device of similar structure (SI Figure S5) but with apparently more defect concentrations, as made evident by its lower device current and more "diode-like" characteristic (SI Figure S5(a)), manifesting further its reproducibility despite the existence of additional defect states or changes in conductivity.

The photovoltaic effect is known to have been caused by the separation of photogenerated electrons and holes through a p-n junction. The collection of these light-generated carriers in the electrodes, at zero external bias, causes the I_{SC}. In contrast, the bias of the p-n junction at zero device current is known as the V_{OC}. The equation, $V_{OC} = \frac{n_d kT}{q}\ln\left(1 + \frac{I_{SC}}{I_0}\right) \approx \frac{n_d kT}{q}\ln\left(\frac{I_{SC}}{I_0}\right)$,[34] relates these two parameters, where n_d is the ideality factor, kT/q the thermal voltage, and I_0 the reverse saturation current. Both parameters are affected by the concentration of electrons and holes in the p-n junction device; hence, V_{OC} can likewise be described in terms of electron and hole concentrations as[35]

$$V_{OC} = \frac{kT}{q}\ln\left(\frac{(N_D + \Delta n)(\Delta p)}{n_i^2}\right) \quad (1)$$

Herein, N_D is the donor concentration of the naturally n-doped CVD-grown MoS_2 on SiO_2/Si substrate (~10^{12} cm^{-2}),[36,37] and n_i the intrinsic concentration (~10^{10} cm^{-2}).[38] Meanwhile, the photogenerated carrier concentrations are expressed as

$$\Delta n = \Delta p = \phi\tau_r = \frac{\eta P_{laser}\lambda}{A_{ph}hc}\tau_r \quad (2)$$

where η is the absorption efficiency, λ the wavelength of the incident light, A_{ph} the illuminated area, h Planck's constant, c the speed of light, τ_r the carrier recombination lifetime, and ϕ

https://doi.org/10.1021/acsnano.1c04902
ACS Nano 2021, 15, 14822−14829

the absorbed photon flux. The above presented experimental results were taken with fixed incident laser power, implying that the temperature on the sample side is almost constant throughout all measurement conditions that is, different OAM of the incident light. The values of the sample's N_D, and n_i can also be considered generally uniform at all measurement conditions. Therefore, the observed improvements in V_{OC} (and also I_{SC}) are likely triggered by the increases in photogenerated carriers, Δn. One can easily illustrate this link between V_{OC} and Δn via the former's direct relationship with the quasi-Fermi level splitting or QFLS (ideally, qV_{OC} = QFLS), as shown in Figure 2(d), which is a term for the reason for mathematical convenience that describes the variations from the equilibrium Fermi level due to the introduction of Δn. Further, as evidenced by the correspondence of the increments of the l of light with the enhancements in V_{OC} (see Figure 2(a),(b)), it can also be deduced that the OAM of light ($l\hbar$) facilitates the increase of Δn on the semiconductor. To support the above-mentioned inferences, simultaneous electrical and optical measurements were performed. Short-circuit current versus time (I-T) pulses (Figure 3(a)), each measured after every increment of the l value of light, were each recorded for 30 s at zero bias voltage. At the same time, three consecutive PL spectra were taken at a fixed power of 20 μW during each I-T pulse. One representative PL spectrum for every instance of the pulse, that is, for each light with positive l, is shown in Figure 3(b). Note that heating effects can be neglected due to the stability of the levels of each current pulse. The rising I_{SC}, along with l, is then revealed to be accompanied by the enhancements of both the MoS_2's integrated PL intensity and the corresponding trion-to-exciton ratio (X^-/X_0) (Figure 3(c)). Interestingly, the observed increases in X^-/X_0 ratio, at incrementing values of l, indicates the progressive improvement of the photogenerated carriers as stated by the law of mass action for charged exciton (trion) formation,[39]

$$n_e = \left(\frac{n_{X^-}}{n_{X_0}}\right)\left(\frac{4m_{\text{eff}}kT}{\pi\hbar^2}\right)e^{-(E_B^{X^-}/kT)} \tag{3}$$

where n_e is the free carrier concentration in the semiconductor, n_{X^-} the trion concentration, n_{X_0} the neutral exciton concentration, m_{eff} the quasiparticle effective mass, $\hbar$ the reduced Planck's constant, and $E_B^{X^-}$ the trion binding energy. The ratio $\frac{n_{X^-}}{n_{X_0}}$ could be replaced with the experimental ratio of the integrated spectral area of trion and exciton , that is, X^-/X_0 (Figure 3(c)), to yield the increasing trend of n_e, and thus Δn, at incrementing values of l. Hence, the optoelectrical analysis above confirms the dependability of the enhancements in our device's V_{OC} and I_{SC} to the improvements in the Δn, and, more importantly, established the OAM ($l\hbar$) of light's control over the levels of Δn. The PL spectra for negative l conditions as well as the detailed peak fitting of all the measured spectra are placed in SI Figures S6 and S7, respectively.

Twisted light was theoretically and experimentally demonstrated to have enhanced the quadrupole (forbidden) transitions in atoms.[9,10] Therein, the total angular momentum of the photon is conserved upon absorption by electrons positioned near the center (dark *penumbra*) of the twisted light beam, where the forbidden transitions are highly activated.[10] Similarly, in semiconductors, such as GaAs, variations in light-generated electron signals were recorded and were attributed to the contributions of the electrons transitioning through the material's twisted-light-activated forbidden transitions.[8] The accounts of these related studies have all suggested that the increase in V_{OC} (and I_{SC}) in the current work might be contributed by virtue of the unlocked forbidden transitions in the MoS_2 material. Through these unlocked transitions, more avenues may be available for photon-absorbing carrier, which leads to the increase in the absorption efficiency, η, and consequently the Δn (see eq 2). This ultimately results to a widening of the QFLS and, in effect, the enhancement of the V_{OC} (Figure 3(d)). It must be noted that the expanding A_{ph} with each increment of the light's $|l|$ (SI Figure S2(b)) has no effect on the material's η as implied by the Beer-Bouguer-Lambert Law. The η at different light conditions *i.e.*, OAM, can be estimated using eqs 1 and 2, however a more precise approximation can be done by considering the enhanced photoconductivity due to the inherent hole trap states in 2D-MoS_2.[40] These trapped holes set up an increase in photoconductivity by an amount equivalent to $q\mu_n p_t$, which can be expressed as an additional term in the equation of photoconductivity, so that $\Delta\sigma = q(\mu_n\Delta n + \mu_p\Delta p) + q\mu_n p_t$, where q is the electron charge, μ_n and μ_p are respectively the electron and hole mobilities, and $p_t = (\phi P_t\tau_r)/\left(\phi\tau_r + P_t\frac{\tau_t}{\tau_g}\right)$ the density of trapped holes.[40] eq 1 can be algebraically modified to consider the effect of trapped holes in MoS_2, resulting to

$$\begin{aligned} n_i^2 e^{qV_{OC}/kT} &= (N_D + \Delta n + p_t)(\Delta p) \\ &= \phi\tau_r N_D + \phi^2\tau_r^2\left(1 + \frac{P_t}{\phi\tau_r + P_t\left(\frac{\tau_t}{\tau_g}\right)}\right) \end{aligned} \tag{4}$$

where

$$\phi = \frac{\eta P_{\text{laser}}\lambda}{A_{ph}hc} \tag{5}$$

Using eqs 4 and 5, noting that ϕ is dependent on the absorption efficiency η, the estimated η was plotted in Figure 3(c). The calculated η, which improves with the $|l|$ of light, were all within the observable range of values in previous studies.[40−42] Details of the calculation can be seen in the SI. Furthermore, the improvements in the integrated PL intensity with respect to the values of l in Figure 3(b) reflects the increasing absorbed photon flux, ϕ, in the material, assuming a fixed PL quantum yield (PLQY), and can be viewed as a manifestation of the improvements in the η. The PLQY is defined as the ratio of the number of photons emitted from the material to the number of photons absorbed ($\text{PLQY} \propto \frac{PL\text{intensity}}{\eta\frac{P_{\text{laser}}}{\hbar\omega}}$). With that said, one can compare the percentage (%) increase with respect to $l = 0$ of the integrated PL intensity (Figure 3(b)) versus that of the previously calculated η (Figure 3(c)), and the result of which is shown in Figure 3(e). The close relationship between the two quantities further evidence the enhancements of η in the MoS_2 device brought about by the increments in l as consistent with the proposed mechanism.

The small yet noticeable differences, however, between the % increases of the integrated PL intensity and the η may be an indication of the presence of other nondominant factors that

https://doi.org/10.1021/acsnano.1c04902
ACS Nano 2021, 15, 14822−14829

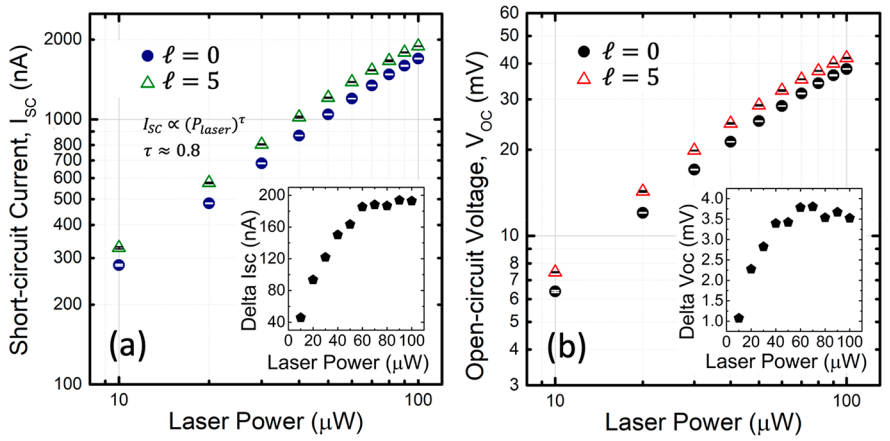

Figure 4. Power-dependence. (a) Short-circuit currents (I_{SC}) and (b) open-circuit voltages (V_{OC}) measured at various incident power of light, carrying $l = 0$ and $l = 5$. The insets of each subfigure show the differences of the values of their respective quantities [I_{SC} in (a) and V_{OC} in (b)] between the $l = 0$ and $l = 5$ conditions with respect to the incident laser power. The error bars are derived from three different measurements in each measurement condition.

could be similarly influenced by the OAM of light on top of the material's η. Referring to SI Figure S7, the narrowing of the trion PL line width at incrementing values of l can be attributed to the improvements of the trion radiative recombination lifetime τ_{Tr}.[43] Based on the relation, PLQY $\propto \frac{1}{\tau_{Tr}}$,[44,45] and the direct relationship of PLQY to the PL intensity, the trion PL intensity is expected to decrease when τ_{Tr} enhances. Hence, the small errors between the two quantities in Figure 3(e) may be due to this OAM-enhanced τ_{Tr} that suppresses trion PL intensity, and thus the integrated PL intensity, especially at higher values of $|l|$. The mechanism supporting the OAM-enhanced τ_{Tr} is yet to be investigated, and a direction that is worthy for further research.

Finally, the laser power-dependent characteristics of the I_{SC} and the V_{OC} in the device is presented in Figure 4(a),(b), respectively. The two parameters behave consistently with other reports,[46] but the difference, or delta, of the values of each of these parameters between two light conditions: $l = 0$ and $l = 5$ (see the insets) gets larger with the incident laser power. This means that the I_{SC} and the V_{OC} at $l = 5$ enhance faster with increasing laser power than in the fundamental mode condition, which is made possible by the increased contributions by the carriers being generated via the supposed unlocked forbidden transitions, as expected. The apparent plateauing of the delta, however, is a sign that OAM-light-excited carriers saturate relatively faster at heightening incident laser power. This saturation behavior at higher excitation intensity could be caused by space-charge effects,[47] which involves a deterioration of carrier velocities and the accumulation of carriers—leading to excess photons not being absorbed. Hence, a more likely reason for the faster saturation at $l = 5$ is the existence of a considerably larger amount of photogenerated carriers in the conduction band, triggering earlier the space-charge effect in the semiconductor.

At present, the study on twisted light and matter interaction is still in its nascent stage and its relevance to solar energy harvesting is not yet entirely clear. Nevertheless, research on ultrathin phase-engineered vortex beam metalenses[48] can lead toward conversion of incident solar energy into twisted light prior to reaching the solar cell. Broadband versions of such metalenses have also been proposed.[49] Hence, further studies invested in these exciting researches coupled with more advanced technology may make twisted light's application to energy harvesting a reality in the near future.

CONCLUSIONS

This work had demonstrated the effectiveness of using twisted light to the properties of photovoltaic devices, such as the monolayer MoS_2 channel device. It was shown that both the V_{OC} and the I_{SC} exhibited enhancements as the l of the incident 532 nm light incremented. Simultaneous optical and electrical measurements showed that the increase in photocurrent, along with l, occurred with an improvement in the trion-to-exciton ratio, which implies enhancements in the photogenerated carrier concentration. Furthermore, it was inferred that the efficiency of the channel material in absorbing incident photons is improved by the OAM of light that may be due to the enhancements of forbidden electronic transitions. The efficiency improvements were estimated and are within the reported experimental values. Finally, the laser power-dependent characteristics of the device's V_{OC} and I_{SC} showed a faster increase of the value of both parameters at $l = 5$ relative to the fundamental mode condition—implying an increased utilization of the supposed unlocked forbidden transitions by the OAM of light with increasing laser power. The findings in this study provide an interesting introduction to the promising capability of the OAM of light in optoelectronic applications. Further studies are expected to branch out as the potential of structured light may be extended from simple device structures to complex heterostructures and solar energy harvesting devices that are designed to take advantage of the light's properties.

METHODS/EXPERIMENTAL

Electrical Characterization and Measurements. Two-terminal electrical measurements were performed using the Keithley 2636B SYSTEM SourceMeter. Electrical measurements were plotted via (a) current versus time (I-T) and (b) current versus bias voltage (I–V) setup. The parameters for both electrical measurements include a 60 s holding time, a 50 ms measurement and source delay times, and at 50 μA compliance. Furthermore, the I-T measurement employs 1000 measurement points at a fixed zero bias voltage.

Parameters of the Spatial Light Modulator (SLM). Plane wave light to twisted light conversion uses a Pluto phase only SLM manufactured by HOLOEYE. The SLM uses the HED 6010 VIS

https://doi.org/10.1021/acsnano.1c04902
ACS Nano 2021, 15, 14822–14829

panel that optimally operates in the 420−700 nm wavelength range with an active area of 0.7 in diagonal (reflective optical mode). In addition, it has a resolution of 1920 × 1080 pixels, a fill factor of 87%, and a pixel pitch of 8 μm.

ASSOCIATED CONTENT

Supporting Information

The Supporting Information is available free of charge at https://pubs.acs.org/doi/10.1021/acsnano.1c04902.

Atomic force microscopy measurement on the monolayer MoS_2 channel; optical setup: Laguerre Gaussian beam generation; electrical measurements on the monolayer MoS_2 while illuminated with light of different OAM conditions; another set of electrical measurements on the monolayer MoS_2 channel device at fixed 100 μW laser power; a set of electrical measurements on the second monolayer MoS_2 channel device at fixed 100 μW optical power; PL measurements on the monolayer MoS_2 using incident light of various OAM; detailed peak fittings of the measured PL spectra; estimating the absorption efficiency (PDF)

AUTHOR INFORMATION

Corresponding Authors

Ting-Hua Lu − *Department of Physics, National Taiwan Normal University, Taipei 11677, Taiwan*; Email: thlu@ntnu.edu.tw

Yann-Wen Lan − *Department of Physics, National Taiwan Normal University, Taipei 11677, Taiwan*; orcid.org/0000-0003-2403-1357; Email: ywlan@ntnu.edu.tw

Authors

Kristan Bryan Simbulan − *Department of Physics, National Taiwan Normal University, Taipei 11677, Taiwan; Department of Mathematics and Physics, University of Santo Tomas, Manila 1008, Philippines*; orcid.org/0000-0001-9102-5876

Yi-Jie Feng − *Department of Physics, National Taiwan Normal University, Taipei 11677, Taiwan*

Wen-Hao Chang − *Department of Physics, National Taiwan University, Taipei 10617, Taiwan*

Chun-I Lu − *Department of Physics, National Taiwan Normal University, Taipei 11677, Taiwan*; orcid.org/0000-0002-7735-1322

Complete contact information is available at: https://pubs.acs.org/10.1021/acsnano.1c04902

Author Contributions

K.B.S. and Y.J.F. performed the experiments/measurements. The data analysis and calculations were done by K.B.S. W.H.C. and C.I.L. fabricated the sample and assisted in building the experimental setup. Y.W.L. and T.H.L. supervised this research. All authors have read and approved the manuscript. All authors discussed the results and commented on the manuscript.

Notes

The authors declare no competing financial interest.

ACKNOWLEDGMENTS

This work was supported by the Ministry of Science and Technology, Taiwan under contract No. MOST 108-2112-M-003-010-MY3 and MOST 108-2112-M-003-009. This work was also in part supported by the Ministry of Education of Taiwan and the Taiwan Semiconductor Research Institute.

REFERENCES

(1) Geisz, J. F.; Steiner, M. A.; Jain, N.; Schulte, K. L.; France, R. M.; McMahon, W. E.; Perl, E. E.; Friedman, D. J. Building a Six-Junction Inverted Metamorphic Concentrator Solar Cell. *IEEE J. Photovoltaics* **2018**, *8* (2), 626−632.

(2) Gul, M.; Kotak, Y.; Muneer, T. Review on Recent Trend of Solar Photovoltaic Technology. *Energy Explor. Exploit.* **2016**, *34* (4), 485−526.

(3) Zakharchenya, B. I.; Fleishe, V. G.; Dzhioev, R. I.; Veshchunov, Y. P.; Rusanov, I. B. Effect of Optical Orientation of Electron Spins in a GaAs Crystal. *JETP Lett.* **1971**, *13* (4), 195−197.

(4) Ekimov, A. I.; Safarov, V. I. Optical Orientation of Carriers in Interband Transitions in Semiconductors. *JETP Lett.* **1970**, *12*, 1−1.

(5) Zeng, H.; Dai, J.; Yao, W.; Xiao, D.; Cui, X. Valley Polarization in MoS_2 Monolayers by Optical Pumping. *Nat. Nanotechnol.* **2012**, *7* (8), 490−493.

(6) Allen, L.; Beijersbergen, M. W.; Spreeuw, R. J. C.; Woerdman, J. P. Orbital Angular Momentum of Light and the Transformation of Laguerre-Gaussian Laser Modes. *Phys. Rev. A: At., Mol., Opt. Phys.* **1992**, *45* (11), 8185−8189.

(7) Fickler, R.; Campbell, G.; Buchler, B.; Lam, P. K.; Zeilinger, A. Quantum Entanglement of Angular Momentum States with Quantum Numbers up to 10,010. *Proc. Natl. Acad. Sci. U. S. A.* **2016**, *113* (48), 13642−13647.

(8) Sordillo, L. A.; Mamani, S.; Sharonov, M.; Alfano, R. R. The Interaction of Twisted Laguerre-Gaussian Light with a GaAs Photocathode to Investigate Photogenerated Polarized Electrons. *Appl. Phys. Lett.* **2019**, *114* (4), 041104.

(9) Schmiegelow, C. T.; Schulz, J.; Kaufmann, H.; Ruster, T.; Poschinger, U. G.; Schmidt-Kaler, F. Transfer of Optical Orbital Angular Momentum to a Bound Electron. *Nat. Commun.* **2016**, *7* (1), 12998.

(10) Babiker, M.; Andrews, D. L.; Lembessis, V. E. Atoms in Complex Twisted Light. *J. Opt.* **2019**, *21* (1), 013001.

(11) Forbes, K. A.; Andrews, D. L. Orbital Angular Momentum of Twisted Light: Chirality and Optical Activity. *J. Phys. Photonics* **2021**, *3* (2), 022007.

(12) Arikawa, T.; Hiraoka, T.; Morimoto, S.; Blanchard, F.; Tani, S.; Tanaka, T.; Sakai, K.; Kitajima, H.; Sasaki, K.; Tanaka, K. Transfer of Orbital Angular Momentum of Light to Plasmonic Excitations in Metamaterials. *Sci. Adv.* **2020**, *6* (24), eaay1977.

(13) Ji, Z.; Liu, W.; Krylyuk, S.; Fan, X.; Zhang, Z.; Pan, A.; Feng, L.; Davydov, A.; Agarwal, R. Photocurrent Detection of the Orbital Angular Momentum of Light. *Science* **2020**, *368* (6492), 763−767.

(14) Tsai, M.-L.; Su, S.-H.; Chang, J.-K.; Tsai, D.-S.; Chen, C.-H.; Wu, C.-I.; Li, L.-J.; Chen, L.-J.; He, J.-H. Monolayer MoS_2 Heterojunction Solar Cells. *ACS Nano* **2014**, *8* (8), 8317−8322.

(15) Hao, L. Z.; Gao, W.; Liu, Y. J.; Han, Z. D.; Xue, Q. Z.; Guo, W. Y.; Zhu, J.; Li, Y. R. High-Performance *n*-MoS_2/i-SiO_2/*p*-Si Heterojunction Solar Cells. *Nanoscale* **2015**, *7* (18), 8304−8308.

(16) Singh, E.; Kim, K. S.; Yeom, G. Y.; Nalwa, H. S. Atomically Thin-Layered Molybdenum Disulfide (MoS_2) for Bulk-Heterojunction Solar Cells. *ACS Appl. Mater. Interfaces* **2017**, *9* (4), 3223−3245.

(17) Xu, Z.-Q.; Zhang, Y.; Wang, Z.; Shen, Y.; Huang, W.; Xia, X.; Yu, W.; Xue, Y.; Sun, L.; Zheng, C.; Lu, Y.; Liao, L.; Bao, Q. Atomically Thin Lateral *p*−*n* Junction Photodetector with Large Effective Detection Area. *2D Mater.* **2016**, *3* (4), 041001.

(18) Pospischil, A.; Furchi, M. M.; Mueller, T. Solar-Energy Conversion and Light Emission in an Atomic Monolayer *p*−*n* Diode. *Nat. Nanotechnol.* **2014**, *9* (4), 257−261.

(19) Choi, M. S.; Qu, D.; Lee, D.; Liu, X.; Watanabe, K.; Taniguchi, T.; Yoo, W. J. Lateral MoS_2 *p*−*n* Junction Formed by Chemical Doping for Use in High-Performance Optoelectronics. *ACS Nano* **2014**, *8* (9), 9332−9340.

(20) Zhong, X.; Zhou, W.; Peng, Y.; Zhou, Y.; Zhou, F.; Yin, Y.; Tang, D. Multi-Layered MoS_2 Phototransistors as High Performance

Photovoltaic Cells and Self-Powered Photodetectors. *RSC Adv.* **2015**, *5* (56), 45239−45248.
(21) Liu, X.; Chen, Y.; Li, D.; Wang, S.-W.; Ting, C.-C.; Chen, L.; Ang, K.-W.; Qiu, C.-W.; Chueh, Y.-L.; Sun, X.; Kuo, H.-C. Nearly Lattice-Matched Molybdenum Disulfide/Gallium Nitride Heterostructure Enabling High-Performance Phototransistors. *Photonics Res.* **2019**, *7* (3), 311.
(22) Kwak, J. Y. Absorption Coefficient Estimation of Thin MoS_2 Film Using Attenuation of Silicon Substrate Raman Signal. *Results Phys.* **2019**, *13*, 102202.
(23) Rajkanan, K.; Singh, R.; Shewchun, J. Absorption Coefficient of Silicon for Solar Cell Calculations. *Solid-State Electron.* **1979**, *22* (9), 793−795.
(24) Liu, J.-T.; Wang, T.-B.; Li, X.-J.; Liu, N.-H. Enhanced Absorption of Monolayer MoS_2 with Resonant Back Reflector. *J. Appl. Phys.* **2014**, *115* (19), 193511.
(25) Long, L.; Yang, Y.; Ye, H.; Wang, L. Optical Absorption Enhancement in Monolayer MoS_2 Using Multi-Order Magnetic Polaritons. *J. Quant. Spectrosc. Radiat. Transfer* **2017**, *200*, 198−205.
(26) Zhou, K.; Song, J.; Lu, L.; Luo, Z.; Cheng, Q. Plasmon-Enhanced Broadband Absorption of MoS_2-Based Structure Using Au Nanoparticles. *Opt. Express* **2019**, *27* (3), 2305.
(27) Bahauddin, S. M.; Robatjazi, H.; Thomann, I. Broadband Absorption Engineering to Enhance Light Absorption in Monolayer MoS_2. *ACS Photonics* **2016**, *3* (5), 853−862.
(28) Zheng, X.; Calò, A.; Cao, T.; Liu, X.; Huang, Z.; Das, P. M.; Drndic, M.; Albisetti, E.; Lavini, F.; Li, T.-D.; Narang, V.; King, W.; Harrold, J.; Vittadello, M.; Aruta, C.; Shahrjerdi, D.; Riedo, E. Spatial Defects Nanoengineering for Bipolar Conductivity in MoS_2. *Nat. Commun.* **2020**, *11* (1), 3463.
(29) Zafar, A.; Nan, H.; Zafar, Z.; Wu, Z.; Jiang, J.; You, Y.; Ni, Z. Probing the Intrinsic Optical Quality of CVD Grown MoS_2. *Nano Res.* **2017**, *10* (5), 1608−1617.
(30) Han, T.; Liu, H.; Wang, S.; Chen, S.; Li, W.; Yang, X.; Cai, M.; Yang, K. Probing the Optical Properties of MoS2 on SiO_2/Si and Sapphire Substrates. *Nanomaterials* **2019**, *9* (5), 740.
(31) Golovynskyi, S.; Irfan, I.; Bosi, M.; Seravalli, L.; Datsenko, O. I.; Golovynska, I.; Li, B.; Lin, D.; Qu, J. Exciton and Trion in Few-Layer MoS_2: Thickness- and Temperature-Dependent Photoluminescence. *Appl. Surf. Sci.* **2020**, *515*, 146033.
(32) Li, H.; Zhang, Q.; Yap, C. C. R.; Tay, B. K.; Edwin, T. H. T.; Olivier, A.; Baillargeat, D. From Bulk to Monolayer MoS_2: Evolution of Raman Scattering. *Adv. Funct. Mater.* **2012**, *22* (7), 1385−1390.
(33) Zhang, Y.; Li, H.; Wang, L.; Wang, H.; Xie, X.; Zhang, S.-L.; Liu, R.; Qiu, Z.-J. Photothermoelectric and Photovoltaic Effects Both Present in MoS_2. *Sci. Rep.* **2015**, *5* (1), 7938.
(34) Li, Z.; Chen, J.; Dhall, R.; Cronin, S. B. Highly Efficient, High Speed Vertical Photodiodes Based on Few-Layer MoS_2. *2D Mater.* **2017**, *4* (1), 015004.
(35) Sinton, R. A.; Cuevas, A. Contactless Determination of Current−Voltage Characteristics and Minority-Carrier Lifetimes in Semiconductors from Quasi-Steady-State Photoconductance Data. *Appl. Phys. Lett.* **1996**, *69* (17), 2510−2512.
(36) Hong, J.; Hu, Z.; Probert, M.; Li, K.; Lv, D.; Yang, X.; Gu, L.; Mao, N.; Feng, Q.; Xie, L.; Zhang, J.; Wu, D.; Zhang, Z.; Jin, C.; Ji, W.; Zhang, X.; Yuan, J.; Zhang, Z. Exploring Atomic Defects in Molybdenum Disulphide Monolayers. *Nat. Commun.* **2015**, *6* (1), 6293.
(37) Chae, W. H.; Cain, J. D.; Hanson, E. D.; Murthy, A. A.; Dravid, V. P. Substrate-Induced Strain and Charge Doping in CVD-Grown Monolayer MoS_2. *Appl. Phys. Lett.* **2017**, *111* (14), 143106.
(38) Wu, C.-C.; Jariwala, D.; Sangwan, V. K.; Marks, T. J.; Hersam, M. C.; Lauhon, L. J. Elucidating the Photoresponse of Ultrathin MoS_2 Field-Effect Transistors by Scanning Photocurrent Microscopy. *J. Phys. Chem. Lett.* **2013**, *4* (15), 2508−2513.
(39) Vercik, A.; Gobato, Y. G.; Brasil, M. J. S. P. Thermal Equilibrium Governing the Formation of Negatively Charged Excitons in Resonant Tunneling Diodes. *J. Appl. Phys.* **2002**, *92* (4), 1888−1892.
(40) Furchi, M. M.; Polyushkin, D. K.; Pospischil, A.; Mueller, T. Mechanisms of Photoconductivity in Atomically Thin MoS_2. *Nano Lett.* **2014**, *14* (11), 6165−6170.
(41) Fang, X.; Tian, Q.; Yang, G.; Gu, Y.; Wang, F.; Hua, B.; Yan, X. Enhanced Absorption of Monolayer Molybdenum Disulfide (MoS_2) Using Nanostructures with Symmetrical Cross Resonator in the Visible Ranges. *Opt. Quantum Electron.* **2019**, *51* (1), 21.
(42) Long, Y.; Deng, H.; Xu, H.; Shen, L.; Guo, W.; Liu, C.; Huang, W.; Peng, W.; Li, L.; Lin, H.; Guo, C. Magnetic Coupling Metasurface for Achieving Broad-Band and Broad-Angular Absorption in the MoS_2 Monolayer. *Opt. Mater. Express* **2017**, *7* (1), 100.
(43) Ajayi, O. A.; Ardelean, J. V.; Shepard, G. D.; Wang, J.; Antony, A.; Taniguchi, T.; Watanabe, K.; Heinz, T. F.; Strauf, S.; Zhu, X.-Y.; Hone, J. C. Approaching the Intrinsic Photoluminescence Linewidth in Transition Metal Dichalcogenide Monolayers. *2D Mater.* **2017**, *4* (3), 031011.
(44) Yuan, L.; Huang, L. Exciton Dynamics and Annihilation in WS_2 2D Semiconductors. *Nanoscale* **2015**, *7* (16), 7402−7408.
(45) Lien, D.-H.; Uddin, S. Z.; Yeh, M.; Amani, M.; Kim, H.; Ager, J. W.; Yablonovitch, E.; Javey, A. Electrical Suppression of All Nonradiative Recombination Pathways in Monolayer Semiconductors. *Science* **2019**, *364* (6439), 468−471.
(46) Wong, J.; Jariwala, D.; Tagliabue, G.; Tat, K.; Davoyan, A. R.; Sherrott, M. C.; Atwater, H. A. High Photovoltaic Quantum Efficiency in Ultrathin van der Waals Heterostructures. *ACS Nano* **2017**, *11* (7), 7230−7240.
(47) Williams, K. J.; Esman, R. D.; Dagenais, M. Effects of High Space-Charge Fields on the Response of Microwave Photodetectors. *IEEE Photonics Technol. Lett.* **1994**, *6* (5), 639−641.
(48) Zhang, K.; Yuan, Y.; Zhang, D.; Ding, X.; Ratni, B.; Burokur, S. N.; Lu, M.; Tang, K.; Wu, Q. Phase-Engineered Metalenses to Generate Converging and Non-Diffractive Vortex Beam Carrying Orbital Angular Momentum in Microwave Region. *Opt. Express* **2018**, *26* (2), 1351.
(49) Mei, S.; Mehmood, M. Q.; Huang, K.; Qiu, C.-W. Multi-Foci Metalens for Spin and Orbital Angular Momentum Interaction. In *Metamaterials, Metadevices, and Metasystems 2015*; Engheta, N., Noginov, M. A., Zheludev, N. I., Eds.; 2015; p 95441J.

https://doi.org/10.1021/acsnano.1c04902
ACS Nano 2021, 15, 14822−14829